

# Electronic noise of warm electrons in semiconductors from first-principles

Alexander Y. Choi ,<sup>1</sup> Peishi S. Cheng ,<sup>1</sup> and Austin J. Minnich  <sup>a1</sup>

<sup>1</sup>*Division of Engineering and Applied Science,  
California Institute of Technology, Pasadena, CA, USA*

(Dated: September 25, 2020)

## Abstract

The *ab-initio* theory of low-field electronic transport properties such as carrier mobility in semiconductors is well-established. However, an equivalent treatment of electronic fluctuations about a non-equilibrium steady state, which are readily probed experimentally, remains less explored. Here, we report a first-principles theory of electronic noise for warm electrons in semiconductors. In contrast with typical numerical methods used for electronic noise, no adjustable parameters are required in the present formalism, with the electronic band structure and scattering rates calculated from first-principles. We demonstrate the utility of our approach by applying it to GaAs and show that spectral features in AC transport properties and noise originate from the disparate time scales of momentum and energy relaxation, despite the dominance of optical phonon scattering. Our formalism enables a parameter-free approach to probe the microscopic transport processes that give rise to electronic noise in semiconductors.

---

<sup>a</sup>Corresponding author: [aminnich@caltech.edu](mailto:aminnich@caltech.edu)

## I. INTRODUCTION

Charge transport in semiconductors is a topic of fundamental and practical interest with a well-established theoretical foundation [1, 2]. In many cases, a sufficient understanding of the relevant physics at both low and high fields can be achieved using the Boltzmann equation with semi-empirical scattering rates [3–6]. In other cases, a more precise description of the electronic transitions induced by phonons and other perturbations is required. Such a description is now possible owing to advances in electronic structure codes that enable the *ab-initio* computation of the transition matrix elements given by Fermi’s golden rule performed in conjunction with the numerical solution of the Boltzmann equation describing carrier dynamics [7–10]. While method development is ongoing, these calculations are now routine for various semiconductors including Si [11–13], GaAs [14–16], phosphorene [7], and others [17–20].

In contrast, an equivalent treatment of fluctuations from a non-equilibrium steady-state is lacking, despite the experimental accessibility of electronic noise [21, 22] and its importance in applications [23]. At equilibrium, the Nyquist relation, or more generally the fluctuation-dissipation theorem, relates the electrical conductivity to the spectral noise power [24–26]. Outside of equilibrium, the theorem no longer applies and the spectral noise power must be computed with another approach.

The theoretical description of fluctuations about a non-equilibrium steady-state has a long history. In 1935, Leontovich used kinetic theory to examine velocity fluctuations of a non-equilibrium gas [27]. Around 20 years later, Wannier established the definition of a diffusion coefficient for transport about a non-equilibrium steady state [28]. Hashitsume considered a microscopic description of occupancy fluctuations about a steady distribution using the Fokker-Planck equation with a random source term [29]. In analogy with earlier works on fluctuational Maxwell equations, Kadomotsev introduced Langevin sources into the Boltzmann equation [30]. Shortly thereafter, Price derived that for spatially homogeneous fluctuations, a fluctuation-diffusion relation links Wannier’s diffusion coefficient to the spectral density of current fluctuations even outside of equilibrium [31]. In the same year, Lax formulated a general kinetic theory of fluctuations for a Markovian system [32]. Throughout the 1960s, Gantsevich and co-workers applied Lax’s kinetic theory to dilute gases for which the evolution of the one particle distribution function is governed by the

linear Boltzmann Equation [33]. Their technique, termed the “method of moments,” demonstrated how to compute the spectral density of current fluctuations using only the solutions of the linear Boltzmann equation. Concurrently with Gantsevich, starting from Kadomtsev’s Boltzmann-Langevin equation, Kogan and Shul’man developed a Langevin treatment of the current density fluctuations [34]. Lax, van Vliet, and Kogan and Shul’man independently confirmed that the method of moments and the Langevin approach are equivalent [35–37].

As computational resources became increasingly available, numerical implementations of the methods described above permitted computations of electronic noise for both warm ( $\Delta T/T_0 \ll 1$ ) and hot ( $\Delta T/T_0 \sim 1$ ) electrons, where  $\Delta T$  is the steady-state temperature rise of the electrons and  $T_0$  is the lattice temperature. Due to the lack of knowledge of the precise transition rates between electronic states, these studies employed simplified band structures and parameterized models for scattering such as deformation potential theory for acoustic phonon scattering [38, 39]. For example, Stanton and Wilkins obtained the Green’s function of the Boltzmann equation under the single-mode relaxation time approximation, demonstrating qualitative agreement with experiment in GaAs for one [40] and two [41] valleys. Numerous Monte Carlo simulations reported calculations of current spectral densities in Si [38, 42–46], GaAs [43, 47, 48], and other semiconductors [49–52]. These works employed various approximations such as Debye acoustic phonons, dispersionless optical phonons, and spherical approximations for electron conduction bands. With empirical knowledge of band structure parameters such as effective mass and approximate relaxation times, reasonable agreement with experiments was reported [38, 42–47, 49, 53, 54]. More recently, these methods have been extended to heterostructures and have provided insight into the design of low noise devices [55–57]. While studies with parameterized models can provide an adequate description of the physics of interest in certain cases, they are not predictive and are restricted to materials for which empirical models of the dominant scattering mechanisms are available. It is therefore natural to consider how advances in the *ab-initio* calculation of mean transport quantities [8, 9] can be applied to the non-equilibrium steady state.

Here, we present an *ab-initio* theory of electronic noise for warm electrons in non-degenerate semiconductors. The formalism provides the spectral noise power and AC transport quantities without any adjustable parameters. Using the method, we show that the anisotropy and spectral features of the noise power in GaAs can be explained by the dis-

parate timescales of momentum and energy exchange with phonons, even though scattering is dominated by the inelastic polar optical phonon scattering mechanism. Our method provides a parameter-free view of the microscopic transport processes responsible for electronic fluctuations in semiconductors and will advance fundamental studies of carrier transport and applications of low noise semiconductor devices.

## II. THEORY

### A. Steady-state transport

We begin by reviewing the *ab-initio* treatment of steady-state transport using the Boltzmann equation to set the notation. Consider a non-degenerate, spatially homogeneous electron gas subject to an external electric field  $\mathcal{E}$ . The field drives the system to a new steady state with distribution  $f_{m\mathbf{k}}^s$  governed by the Boltzmann equation:

$$\frac{e\mathcal{E}_\gamma}{\hbar} \partial_{k_\gamma} f_{m\mathbf{k}}^s + \mathcal{I}[f_{m\mathbf{k}}^s] = 0 \quad (1)$$

Here,  $f_{m\mathbf{k}}^s$  is the steady-state distribution function that describes the occupancy of the quantum state with wave vector  $\mathbf{k}$  and band index  $m$ ,  $e$  is the fundamental charge,  $\hbar$  is the reduced Planck constant, and  $\gamma = x, y, z$  indexes the crystal axes. In the above and following expressions, repeated indices imply summation. The collision integral,  $\mathcal{I}$ , describes the scattering rates between electronic Bloch states  $m\mathbf{k}$  and  $m'\mathbf{k}'$ . In general, the collision integral is a nonlinear functional of the distribution function. Taking electron-phonon scattering as the dominant scattering mechanism, the nonlinear collision integral is given by Fermi's Golden Rule [1].

In many problems, a good approximation is that the Boltzmann equation can be linearized about an equilibrium distribution as  $f_{m\mathbf{k}}^s \equiv f_{m\mathbf{k}}^0 + \Delta f_{m\mathbf{k}}$ , where  $\Delta f_{m\mathbf{k}}$  is the change in occupation due to the electric field  $\mathcal{E}$  relative to the equilibrium distribution  $f_{m\mathbf{k}}^0$ . Under the non-degenerate assumption,  $f_{m\mathbf{k}}^0$  is well approximated by the Maxwell-Boltzmann distribution. With this substitution and retaining only terms linear in  $\Delta f_{m\mathbf{k}}$ , the Boltzmann equation becomes [3]:

$$\frac{e\mathcal{E}_\gamma}{\hbar} \partial_{k_\gamma} \Delta f_{m\mathbf{k}} + \Theta_{m\mathbf{k}m'\mathbf{k}'} \Delta f_{m'\mathbf{k}'} = -\frac{e\mathcal{E}_\gamma}{\hbar} \partial_{k_\gamma} f_{m\mathbf{k}}^0 \quad (2)$$

and  $\Theta_{m\mathbf{k}m'\mathbf{k}'}$  is the linearized collision integral:

$$\Theta_{m\mathbf{k}m'\mathbf{k}'} = -\frac{2\pi}{N\hbar} \sum_{m'\nu\mathbf{q}} |g_{m\mathbf{k},m'\mathbf{k}+\mathbf{q}}|^2 \left[ \delta(\epsilon_{m\mathbf{k}} - \hbar\omega_{\nu\mathbf{q}} - \epsilon_{m'\mathbf{k}+\mathbf{q}}) H_{em} + \delta(\epsilon_{m\mathbf{k}} + \hbar\omega_{\nu\mathbf{q}} - \epsilon_{m'\mathbf{k}+\mathbf{q}}) H_{abs} \right] \quad (3)$$

Here,  $g_{m\mathbf{k},m'\mathbf{k}'}$  is the matrix element coupling electron state  $m\mathbf{k}$  to another electron state  $m'\mathbf{k}' = m'\mathbf{k} + \mathbf{q}$  via emission or absorption of a phonon with wave vector  $\mathbf{q}$ , polarization  $\nu$ , and occupancy  $N_{\nu\mathbf{q}}$  given by the Bose distribution.  $N$  is the total number of  $\mathbf{q}$ -points. The linearized emission and absorption weights are  $H_{ems} = N_{\mathbf{q}} + 1 - f_{m\mathbf{k}+\mathbf{q}}^0$  and  $H_{abs} = N_{\mathbf{q}} + f_{m\mathbf{k}+\mathbf{q}}^0$ , respectively, if  $m'\mathbf{k}' = m\mathbf{k}$ , and  $H_{ems} = -(N_{\mathbf{q}} + f_{m\mathbf{k}}^0)$  and  $H_{abs} = -(N_{\mathbf{q}} + 1 - f_{m\mathbf{k}}^0)$  if  $m'\mathbf{k}' \neq m\mathbf{k}$ .

In the present study, we restrict the electric field to values where  $\Delta f_{m\mathbf{k}} \ll f_{m\mathbf{k}}^0$  so that the linearization above is valid. However, in the typical *ab-initio* treatment of transport, the electric field is further assumed to be small enough such that  $\partial_{k_\gamma} f_{m\mathbf{k}} \approx \partial_{k_\gamma} f_{m\mathbf{k}}^0$ , allowing  $\Delta f_{m\mathbf{k}}$  to be obtained by an iterative method with only knowledge of  $\Theta_{m\mathbf{k}m'\mathbf{k}'}$  and the equilibrium distribution  $f_{m\mathbf{k}}^0$  [8]. In the present problem, the field is sufficiently large such that  $\partial_{k_\gamma} \Delta f_{m\mathbf{k}} \sim \partial_{k_\gamma} f_{m\mathbf{k}}^0$  and the neglected derivative term,  $\partial_{k_\gamma} \Delta f_{m\mathbf{k}}$ , must be included. This approximation was originally denoted as the ‘warm electron’ approximation since the excess energy of the electrons over the thermal value can be non-zero while remaining small on that scale [6].

To treat the drift term numerically, we employ a finite difference approximation:

$$\frac{e\mathcal{E}_\gamma}{\hbar} \partial_{k_\gamma} \Delta f_{m\mathbf{k}}^s \approx \frac{e\mathcal{E}_\gamma}{\hbar} D_{m\mathbf{k}m'\mathbf{k}',\gamma} \Delta f_{m'\mathbf{k}'} \quad (4)$$

where the momentum-space derivative is approximated using a first-order central difference scheme:

$$D_{m\mathbf{k}m'\mathbf{k}',\gamma} = \frac{\delta_{mk_\gamma, mk_\gamma + \Delta k_\gamma} - \delta_{mk_\gamma, mk_\gamma - \Delta k_\gamma}}{2\Delta k_\gamma} \quad (5)$$

Here,  $\delta_{i,j}$  is the Kronecker delta function and  $\Delta k_\gamma$  is the wave vector spacing of the reciprocal space mesh along the  $\gamma$  crystal axis. The drift operator requires boundary conditions that will be given in Section III.

With these definitions, the steady Boltzmann equation becomes:

$$\Lambda_{m\mathbf{k}m'\mathbf{k}'} \Delta f_{m'\mathbf{k}'} \equiv \left[ \frac{e\mathcal{E}_\gamma}{\hbar} D_{m\mathbf{k}m'\mathbf{k}',\gamma} + \Theta_{m\mathbf{k}m'\mathbf{k}'} \right] \Delta f_{m'\mathbf{k}'} = \frac{e\mathcal{E}_\gamma}{k_B T} v_{m\mathbf{k},\gamma} f_{m\mathbf{k}}^0 \quad (6)$$

Here, we have analytically expanded the gradient of the equilibrium Boltzmann distribution on the right-hand side as  $\partial_{k_\gamma} f_{m\mathbf{k}}^0 = -(\hbar v_{m\mathbf{k},\gamma}/k_B T) f_{m\mathbf{k}}^0$ , where  $v_{m\mathbf{k}}$  is the group velocity and  $k_B T$  is the thermal energy.  $\Lambda_{m\mathbf{k}m'\mathbf{k}'}$  is defined as the relaxation operator that combines the drift and scattering operators. Equation 6 shows that the steady Boltzmann equation is now a system of linear equations. The solution,  $\Delta f_{m\mathbf{k}}$ , can be written symbolically using the inverse relaxation operator:

$$\Delta f_{m\mathbf{k}} = \Lambda_{m\mathbf{k}m'\mathbf{k}'}^{-1} \left( \frac{e\mathcal{E}_\gamma}{k_B T} \right) v_{m'\mathbf{k}',\gamma} f_{m'\mathbf{k}'}^0 \quad (7)$$

Transport properties such as the electrical conductivity can be defined using the steady distribution. In particular, the DC conductivity  $\sigma_{\alpha\beta}^{eq}$  can be expressed as:

$$\sigma_{\alpha\beta}^{eq} = \frac{2e^2}{k_B T \mathcal{V}_0} \sum_{m\mathbf{k}} v_{m\mathbf{k},\alpha} \Theta_{m\mathbf{k}m'\mathbf{k}'}^{-1} v_{m'\mathbf{k}',\beta} f_{m'\mathbf{k}'}^0 \quad (8)$$

where the factor of 2 accounts for spin degeneracy,  $\mathcal{V}_0$  is the supercell volume, and  $\alpha$  and  $\beta$  are the axes along which the current is measured. The conductivity of Eqn. 8, which has been frequently reported in the literature, is typically calculated for a cold electron population with the implicit assumption that  $\partial_{k_\gamma} \Delta f_{m\mathbf{k}} \ll \partial_{k_\gamma} f_{m\mathbf{k}}^0$  and is thus independent of the electric field.

For sufficiently large fields that  $\partial_{k_\gamma} \Delta f_{m\mathbf{k}} \sim \partial_{k_\gamma} f_{m\mathbf{k}}^0$ , the DC conductivity depends on the electric field and is defined with the relaxation operator:

$$\sigma_{\alpha\beta}(\mathcal{E}) = \frac{2e^2}{k_B T \mathcal{V}_0} \sum_{m\mathbf{k}} v_{m\mathbf{k},\alpha} \Lambda_{m\mathbf{k}m'\mathbf{k}'}^{-1} v_{m'\mathbf{k}',\beta} f_{m'\mathbf{k}'}^0 \quad (9)$$

Another important transport quantity, the AC small-signal conductivity  $\sigma_{\alpha\beta}^\omega$ , describes the linear response of the system about a non-equilibrium steady-state [21]. With the steady distribution  $f_{m\mathbf{k}}^s$  being set by a DC field  $\mathcal{E}$  as described above, an AC field perturbation along crystal axis  $\gamma$ ,  $\delta\mathcal{E}_\gamma(t) = \delta\mathcal{E}_\gamma e^{-i\omega t}$ , induces a fluctuation of the steady distribution  $\delta f_{m\mathbf{k}}(t) = \delta f_{m\mathbf{k}}(\omega) e^{-i\omega t}$ . This fluctuation is governed by the Fourier transformed Boltzmann equation:

$$(-i\omega \mathbb{I} + \Lambda)_{m\mathbf{k}m'\mathbf{k}'} \delta f_{m'\mathbf{k}'} = -\frac{e\delta\mathcal{E}_\gamma}{\hbar} \partial_{k_\gamma} f_{m\mathbf{k}}^s \quad (10)$$

Here,  $\mathbb{I}$  is the identity matrix. The fluctuation in the distribution function induces a current fluctuation about the DC value, given as:

$$\delta j_\alpha = \frac{2e}{\mathcal{V}_0} \sum_{m\mathbf{k}} v_{m\mathbf{k},\alpha} \delta f_{m\mathbf{k}} \quad (11)$$

The small-signal AC conductivity is defined as the linear coefficient relating the current density variation to the perturbation,  $\sigma_{\alpha\beta}^\omega \equiv \delta j_\alpha / \delta \mathcal{E}_\beta$ . An explicit expression for AC conductivity can be obtained by combining the above expressions:

$$\sigma_{\alpha\beta}^\omega = \frac{2e^2}{\hbar\mathcal{V}_0} \sum_{m\mathbf{k}} v_{m\mathbf{k},\alpha} (-i\omega \mathbb{I} + \Lambda)_{m\mathbf{k}m'\mathbf{k}'}^{-1} (-\partial_{k'_\beta} f_{m'\mathbf{k}'}^s) \quad (12)$$

At equilibrium the steady distribution reduces to the equilibrium distribution  $f_{m\mathbf{k}}^s = f_{m\mathbf{k}}^0$ , the kinetic operator reduces to the scattering operator,  $\Lambda_{m\mathbf{k}m'\mathbf{k}'} = \Theta_{m\mathbf{k}m'\mathbf{k}'}$ . By examining Eq. 8 and Eq. 12, we see that at equilibrium the zero-frequency differential conductivity is equal to the linear DC conductivity  $\sigma_{\alpha\beta}^{\omega=0}(\mathcal{E} = 0) = \sigma_{\alpha\beta}^{eq}$ .

## B. Fluctuations about a non-equilibrium steady state

We now consider fluctuations about a non-equilibrium steady state induced by the stochastic nature of charge carrier scattering. Consider now that the steady state distribution  $f_{m\mathbf{k}}^s$  is known. Just as in equilibrium, fluctuations in the instantaneous occupation of the quantum states occur. Microscopically, these fluctuations arise because of the stochastic nature of the scattering described by  $\Theta_{m\mathbf{k}m'\mathbf{k}'}$ . At steady state, detailed balance requires that the mean flux of particles into every quantum state is zero. However, the flux of particles into or out of a quantum state is a Poissonian process and is characterized by a variance. Therefore, the instantaneous net flux into a quantum state is in general non-zero due to instantaneous imbalance between the incoming and outgoing fluxes [58]. Consequently, the occupancy of quantum states fluctuates under both equilibrium and non-equilibrium conditions.

In the macroscopic limit at which fluctuations are observed in the laboratory, these distribution function fluctuations appear as instantaneous current fluctuations, or equivalently,

as electronic noise. A non-random characteristic of these fluctuations is the spectral density of current density fluctuations, which, by the Wiener-Khintchine Theorem, is related to the single-sided Fourier transform of the autocorrelation of the current density fluctuations [21]:

$$S_{j_\alpha j_\beta}(\omega) \equiv (\delta j_\alpha \delta j_\beta)_\omega = 2 \int_{-\infty}^{\infty} \overline{\delta j_\alpha(t) \delta j_\beta} e^{-i\omega t} dt \quad (13)$$

where the overbar indicates ensemble average.

We seek to link the macroscopic current density fluctuations to microscopic distribution function fluctuations. Following Ref. [58], we now consider random fluctuations about the non-equilibrium steady state,  $\delta f_{m\mathbf{k}}(t) = f_{m\mathbf{k}}(t) - f_{m\mathbf{k}}^s$ . In contrast to the fluctuations associated with the small signal conductivity, these fluctuations are induced by the stochastic nature of scattering rather than an external perturbation. The corresponding current density fluctuations can be expressed in terms of the fluctuation in the distribution function as in Eqn. 11.

It follows that the ensemble average of the correlation function of instantaneous current fluctuations along axes  $\alpha$  and  $\beta$ ,  $\overline{\delta j_\alpha(t) \delta j_\beta}$ , can be expressed in terms of the correlation function of the occupancy fluctuations,  $\overline{\delta f_{m\mathbf{k}}(t) \delta f_{m_1\mathbf{k}_1}}$ :

$$\overline{\delta j_\alpha(t) \delta j_\beta} = \left( \frac{2e}{V_0} \right)^2 \sum_{m\mathbf{k}} \sum_{m_1\mathbf{k}_1} v_{m\mathbf{k}, \alpha} v_{m_1\mathbf{k}_1, \beta} \overline{\delta f_{m\mathbf{k}}(t) \delta f_{m_1\mathbf{k}_1}} \quad (14)$$

Equation 14 shows that computing the spectral density of current density fluctuations requires calculating the correlations of single particle occupancy fluctuations  $\overline{\delta f_{m\mathbf{k}}(t) \delta f_{m_1\mathbf{k}_1}}$ . This function is known as the time-displaced, two particle correlation function [58]. Through a quantum statistical mechanical treatment, Gantsevich and coauthors have demonstrated that the time-displaced, two particle correlation function obeys the same Boltzmann equation as the fluctuation itself: [33]

$$\frac{\partial}{\partial t} \overline{\delta f_{m\mathbf{k}}(t) \delta f_{m_1\mathbf{k}_1}} + \Lambda_{m\mathbf{k} m'\mathbf{k}'} \overline{\delta f_{m'\mathbf{k}'}(t) \delta f_{m_1\mathbf{k}_1}} = 0 \quad (15)$$

The result of Eqn. 15 can also be justified less mathematically rigorously but with more physical intuition from Onsager's regression hypothesis (in particular, see Sec. 1 of [58]).

Solving Eqn. 15 requires specifying an initial condition,  $\overline{\delta f_{m'\mathbf{k}'} \delta f_{m_1\mathbf{k}_1}}$ , which is known as the one-time, two-particle correlation function. For a non-degenerate system with a fixed number of particles  $N$ , Fowler [59] and Lax [32] derived the required condition as:

$$\overline{\delta f_{m\mathbf{k}} \delta f_{m_1\mathbf{k}_1}} = f_{m\mathbf{k}} \delta_{\mathbf{kk}_1} \delta_{mm_1} - \frac{f_{m\mathbf{k}} f_{m_1\mathbf{k}_1}}{N} \quad (16)$$

where the second term on the right-hand side indicates that a correlation exists between occupancies due to the fixed particle number. With this initial condition for the correlation, Eqns. 13, 14, and 15 can be combined to express the spectral density of current fluctuations explicitly in terms of solutions to the Boltzmann equation. For a single band, we drop the band index to get:

$$(\delta j_\alpha \delta j_\beta)_\omega = \left( \frac{2e}{\mathcal{V}_0} \right)^2 \sum_{\mathbf{k}, \mathbf{k}_1} v_{\mathbf{k}, \alpha} v_{\mathbf{k}_1, \beta} (\delta f_{\mathbf{k}} \delta f_{\mathbf{k}_1})_\omega \quad (17)$$

As with the current density, the spectral density of distribution function fluctuations is related to its analogous correlation function by Fourier transform:

$$(\delta f_{\mathbf{k}} \delta f_{\mathbf{k}_1})_\omega = \int_{-\infty}^{\infty} \overline{\delta f_{\mathbf{k}}(t) \delta f_{\mathbf{k}_1}} e^{-i\omega t} dt \quad (18)$$

By exploiting the stationary property of the autocorrelation function, the spectral density can be expressed as [58]:

$$(\delta f_{\mathbf{k}} \delta f_{\mathbf{k}_1})_\omega = 2\Re \left[ (-i\omega \mathbb{I} + \Lambda)_{\mathbf{k}\mathbf{k}'}^{-1} \overline{\delta f_{\mathbf{k}'} \delta f_{\mathbf{k}_1}} \right] \quad (19)$$

Combining Eqns. 16, 17, and 19 we obtain the following expression:

$$\begin{aligned} S_{j_\alpha j_\beta}(\omega) &= 2 \left( \frac{2e}{\mathcal{V}_0} \right)^2 \Re \left[ \sum_{\mathbf{k}} v_{\mathbf{k}, \alpha} (-i\omega \mathbb{I} + \Lambda)_{\mathbf{k}\mathbf{k}'}^{-1} \sum_{\mathbf{k}_1} v_{\mathbf{k}_1, \beta} \left( f_{\mathbf{k}'}^s \delta_{\mathbf{k}'\mathbf{k}_1} - \frac{f_{\mathbf{k}'}^s f_{\mathbf{k}_1}^s}{N} \right) \right] \\ &= 2 \left( \frac{2e}{\mathcal{V}_0} \right)^2 \Re \left[ \sum_{\mathbf{k}} v_{\mathbf{k}, \alpha} (-i\omega \mathbb{I} + \Lambda)_{\mathbf{k}\mathbf{k}'}^{-1} \left( f_{\mathbf{k}'}^s (v_{\mathbf{k}', \beta} - V_\beta) \right) \right] \end{aligned} \quad (20)$$

Here,  $V_\beta$  is the drift velocity along the  $\beta$  axis defined as:

$$V_\beta = \frac{1}{N} \sum_{\mathbf{k}} v_{\mathbf{k}, \beta} f_{\mathbf{k}}^s \quad (21)$$

where  $N = \sum_{\mathbf{k}} f_{\mathbf{k}}$  is the total particle number.

From Eqn. 20, it follows that calculating the spectral density of the current fluctuations requires solving the inhomogeneous Boltzmann equation twice. First, the steady occupation function must be obtained using Eqn. 7. Then, the Boltzmann equation is solved again with

inhomogeneous term  $f_{\mathbf{k}}^s(v_{\mathbf{k},\beta} - V_\beta)$  with  $f_{m\mathbf{k}}^s \equiv f_{m\mathbf{k}}^0 + \Delta f_{m\mathbf{k}}$ . The appropriate Brillouin zone integrations are then performed to calculate the power spectral density.

As a check of the above derivation, consider an equilibrium system for which  $\mathcal{E}_\gamma = 0$  and  $V_\gamma = 0$ . The equation is simplified as  $f_{\mathbf{k}}^s = f_{\mathbf{k}}^0$  and  $\Lambda_{\mathbf{k}\mathbf{k}'} = \Theta_{\mathbf{k}\mathbf{k}'}$ . Then, we have:

$$S_{j_\alpha j_\beta}(\mathcal{E} = 0) = 2 \left( \frac{2e}{\mathcal{V}_0} \right)^2 \Re \left[ \sum_{\mathbf{k}} v_{\mathbf{k},\alpha} (-i\omega \mathbb{I} + \Theta)_{\mathbf{k}\mathbf{k}'}^{-1} f_{\mathbf{k}'}^0 v_{\mathbf{k}',\beta} \right] \quad (22)$$

With the same simplifications, the equilibrium AC conductivity is:

$$\sigma_{\alpha\beta}^\omega(\mathcal{E} = 0) = -\frac{2e^2}{\hbar\mathcal{V}_0} \sum_{\mathbf{k}} v_{\mathbf{k},\alpha} (-i\omega \mathbb{I} + \Theta)_{\mathbf{k}\mathbf{k}'}^{-1} \partial_{k'_\beta} f_{\mathbf{k}'}^0 \quad (23)$$

Combining the above expressions, we obtain the familiar Nyquist relationship [26]:

$$S_{j_\alpha j_\beta}(\mathcal{E} = 0) = 4 \frac{k_B T_0}{\mathcal{V}_0} \Re[\sigma_{\alpha\beta}^\omega(\mathcal{E} = 0)] \quad (24)$$

This relationship is formally valid only in equilibrium but remains approximately true in the ‘cold’ electron regime for which  $\partial_{\mathbf{k}} f_{m\mathbf{k}}^s \approx \partial_{\mathbf{k}} f_{m\mathbf{k}}^0$  and  $\Delta f_{m\mathbf{k}} \ll f_{m\mathbf{k}}^0$  such that  $\Lambda_{\mathbf{k}\mathbf{k}'} \approx \Theta_{\mathbf{k}\mathbf{k}'}$  and  $f_{m\mathbf{k}}^s \approx f_{m\mathbf{k}}^0$ .

### III. NUMERICAL METHODS

We now describe how to compute the spectral noise power and other quantities using the theory from the previous section. The inputs to the Boltzmann equation are the electronic structure and electron-phonon matrix elements  $g_{m\mathbf{k},m'\mathbf{k}+\mathbf{q}}$  calculated using electronic structure packages. First, the electronic structure and electron-phonon matrix elements are computed on a coarse  $8 \times 8 \times 8$  grid using density functional theory (DFT) and density functional perturbation theory (DFPT), respectively, with QUANTUM ESPRESSO (QE) [60, 61]. These quantities are then interpolated to finer grids using Wannier interpolation with PERTURBO [62]. PERTURBO includes corrections for polar materials, which are necessary in GaAs [63]. Currently, PERTURBO accounts for first-order  $e$ -ph (1ph) processes, and thus only these processes are included in the present work. Higher-order interactions are known to be significant in GaAs [16]. Our method will be extended to incorporate these contributions in a future work.

The electronic structure calculations using QE employ the same simulation parameters as in Ref. [64]. In brief, we use a plane wave cutoff of 72 Ryd and a relaxed lattice parameter of 5.556 Å. We set the Fermi level to obtain a carrier concentration of  $10^{15}$  cm $^{-3}$  corresponding to a non-degenerate electron gas. We consider only conduction band electronic states within an energy cutoff of 300 meV above the conduction band minimum (CBM). This energy window is larger than the window used in typical electron transport calculations since the present calculations allow the electric field to heat the electrons, leading to occupation at higher energy states. Further increasing the energy window by 50 meV had negligible effect on the observables of interest like spectral noise power.

In PERTURBO, we use a grid of  $200 \times 200 \times 200$  for the Wannier interpolated electronic structures and electron-phonon matrix elements. We consider convergence by determining the change in the spectral noise power at the maximum electric field where the  $\Delta f_{m\mathbf{k}} \ll f_{m\mathbf{k}}^0$  assumption is satisfied. Numerical experimentation shows that this condition is satisfied for  $\mathcal{E} \lesssim 500$  V cm $^{-1}$ . The spectral noise power at 500 V cm $^{-1}$  using the  $200 \times 200 \times 200$  grid differs by less than 1% from the value obtained on a grid with twice the number of grid points. The delta function in the electron-phonon matrix elements is approximated with a Gaussian with a 10 meV broadening parameter [64]. Decreasing the broadening to 6 meV changed the spectral noise power at 500 V cm $^{-1}$  by less than 3%.

While PERTURBO performs the Wannier interpolation for the electron-phonon interaction on fine grids, it does not explicitly construct the collision matrix of Eqn. 3. Instead, the mobility is computed using an iterative scheme under the ‘cold’ electron approximation [8]. We found that this iterative method was numerically unstable for the warm electron case. We instead solved the linear system using the Generalized Minimal Residual (GMRES) algorithm as implemented in the Scientific Python library [65]. The matrix was constructed by modifying PERTURBO to output the elements of Eqn. 3.

As described in Sec. II, the derivative term corresponding to particle drift in an electric field  $\mathcal{E}$  is approximated by a finite difference matrix. While the interior entries of this matrix are given by Eqn. 5, boundary conditions must be applied due to the first-order partial derivative. Assuming for concreteness that the electric field is applied along the  $x$  crystal axis, one boundary condition must be specified for every  $k_y$  and  $k_z$  pair. For a given  $k_y$  and  $k_z$  pair, we set the the electron state with the highest energy in the associated  $x$  axis to have zero occupation by removing the contributions of these states to the finite difference

matrix. Explicitly, we remove the  $\delta_{mk_x, mk_x - \Delta k_x}$  term in the central difference scheme of Eqn. 5 when the state with wave vector  $mk_x - \Delta k_x$  is the highest energy state. The energy window is selected so that these highest energy states indeed have negligible population, also ensuring that scattering induced by the collision matrix  $\Theta_{m\mathbf{k}m'\mathbf{k}'}$  for these states can be neglected.

With the collision and drift matrices computed, we then construct the relaxation operator  $\Lambda_{m\mathbf{k}m'\mathbf{k}'}$ , Eqn. 6. The steady-state distribution is obtained by solving the resulting linear system given by Eqn. 7. We then solve Eqn. 20 with the inhomogenous term constructed from the previously computed steady-state distribution as input. For this second Boltzmann equation, we include an  $-i\omega$  term on the diagonal of the linear system which corresponds to the Fourier transformed time derivative. Finally, the spectral density is computed as a Brillouin zone integration over the resulting distribution. The calculation of the AC mobility proceeds in a similar way as for the steady distribution except with the addition of the  $-i\omega$  term.

## IV. RESULTS

### A. Transport

We begin by examining the steady state distribution and associated transport observables in the cold and warm electron regimes. Figure 1a compares the difference between the steady state distribution functions under the two approximations versus wave vector parallel to the electric field,  $k_x$ . We henceforth refer to this direction as the longitudinal direction. At low fields  $\mathcal{E} < 100 \text{ V cm}^{-1}$ , the solutions are nearly identical, but as the field increases, differences in the distribution functions emerge. Under the cold electron approximation, Eqn. 7 shows that  $\Delta f_{m\mathbf{k}}$  is required to possess odd symmetry about the Brillouin zone center because  $\partial_{\mathbf{k}} f_{m\mathbf{k}}^0$  is odd with respect to  $k_x$  while the scattering matrix is even ( $\Theta_{\mathbf{k}\mathbf{k}'} = \Theta_{-\mathbf{k}-\mathbf{k}'}$ ); this symmetry is evident in Fig. 1a. In contrast, in the warm electron case the electrons can be heated and the solution becomes asymmetric with increasing field.

The transport properties of the warm electron distribution differ from those of the cold distribution because warm electrons in the high energy tail are able to emit optical phonons and hence exhibit higher scattering rates. The DC mobility under the two approximations

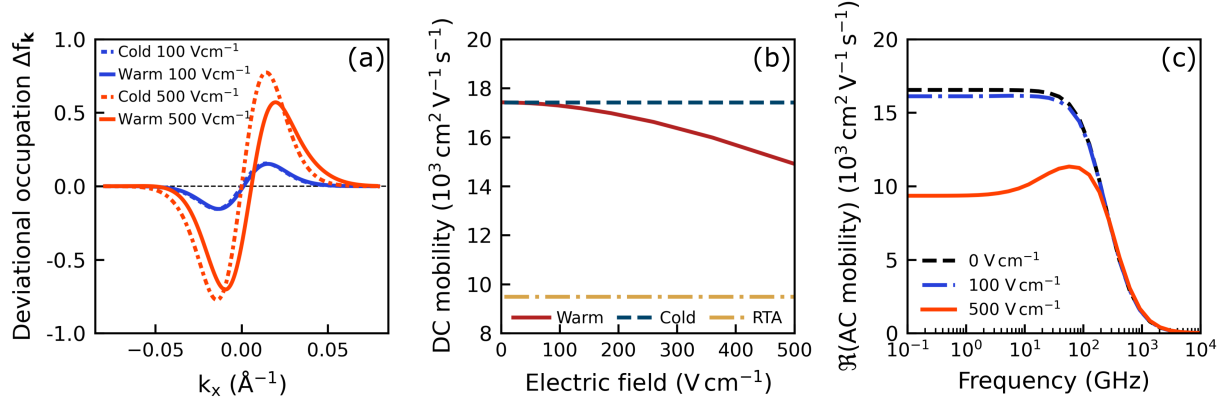


Figure 1. (a) Deviational occupation  $\Delta f_k$  in GaAs at 300 K under the cold (dotted lines) and warm (solid lines) electron approximations versus longitudinal wave vector  $k_x$ . Curves plotted for  $\mathcal{E} = 100 \text{ V cm}^{-1}$  (blue), and  $\mathcal{E} = 500 \text{ V cm}^{-1}$  (orange). (b) Longitudinal ( $\parallel$ ) DC mobility versus electric field of the cold (dashed blue line) and warm electrons (solid red line) along with the RTA mobility (dash-dot yellow line). The heating of the electrons leads to a decreased mobility. (c) Real part of the longitudinal small-signal AC mobility versus frequency for equilibrium (dashed black line),  $\mathcal{E} = 100 \text{ V cm}^{-1}$  (dash-dot blue line), and  $\mathcal{E} = 500 \text{ V cm}^{-1}$  (solid orange line) under the warm electron approximation. The AC mobility exhibits spectral features at frequencies that are characteristic of the inverse momentum and energy relaxation times (see Section IV C).

and the cold electron RTA mobility is shown in Fig. 1b. As has been reported previously, the DC mobility in GaAs from solving the full BTE is greater than that of the RTA mobility [15, 62]. At low fields  $\mathcal{E} < 100 \text{ V cm}^{-1}$ , the mobility under the two approximations agrees to within 1%. At  $\mathcal{E} = 500 \text{ V cm}^{-1}$ , the DC mobility of the warm electrons has decreased by more than 10%. This behavior is qualitatively consistent with the sublinear current voltage characteristic (CVC) of n-type GaAs [21], or a decrease in mobility with increasing electron temperature. More quantitatively, the absolute value of the cold electron mobility is known to be overestimated in the present treatment owing to a lack of higher-order phonon scattering processes [16], preventing an absolute direct comparison with the mobility at higher fields. Focusing on the trend with electric field, the predicted dependence of the mobility appears to be slightly overestimated as well, with the experimental mobility varying weakly with electric field [6, 66]. This discrepancy may also be due to the lack of higher-order scattering processes in the present work and will be investigated in a future work.

In addition to steady quantities, the small-signal AC mobility can be computed as in Eqn. 12. Figure 1c presents the small-signal AC mobility for the warm electron gas versus frequency for several electric fields. At zero frequency, comparison to Fig. 1b demonstrates that the equilibrium AC mobility is equal to the equilibrium DC mobility, as expected. The decrease of the AC mobility with electric field at is also consistent with the trend observed in the DC mobility. At  $f \sim 1$  THz, the AC field frequency exceeds the phonon-mediated scattering rates which redistribute the electrons, and thus the AC mobility rolls off at all fields. This result reflects the electrical response transitioning from a purely resistive to a purely reactive regime as the frequency exceeds highest scattering rate of the system.

The frequency dependence of the AC mobility indicates the relevant timescales of momentum and energy relaxation [67]. In particular, for  $500$  V cm $^{-1}$ , we observe a lower value of the AC mobility at low frequency, followed by a maximum at around 100 GHz. This feature is due to energy exchange with phonons and will be discussed in Section IV C.

## B. Low frequency noise

We now calculate the spectral density of current fluctuations from the non-equilibrium steady state in GaAs. Figure 2a shows the spectral density of longitudinal current fluctuations versus electric field at an observation frequency of 1 MHz, far smaller than any scattering rate. At equilibrium, the noise is given by the Nyquist relation, Eqn. 24. It is conventional to report the spectral density normalized to the Nyquist value to allow comparison between samples of different carrier density [22].

As the electric field increases, the computed noise decreases below the Nyquist value. Few experimental studies of noise in GaAs cover the fields of present interest, but reasonable agreement is observed with a measurement by Bareikis and coauthors [68]. We note that a similar decrease with field is observed in other studies in GaAs [69, 70] though the sparsity of data in the relevant electric field range prevents direct comparison.

To better understand the decreasing trend, we use an approximate solution of the Boltzmann equation for an electron gas interacting quasi-elastically with a thermal phonon bath [24, 66]. Under the quasi-elastic approximation, the distribution function is expanded in momentum space using Legendre polynomials. Because the distribution is nearly isotropic in momentum space under quasi-elastic scattering, only the two lowest Legendre polynomi-

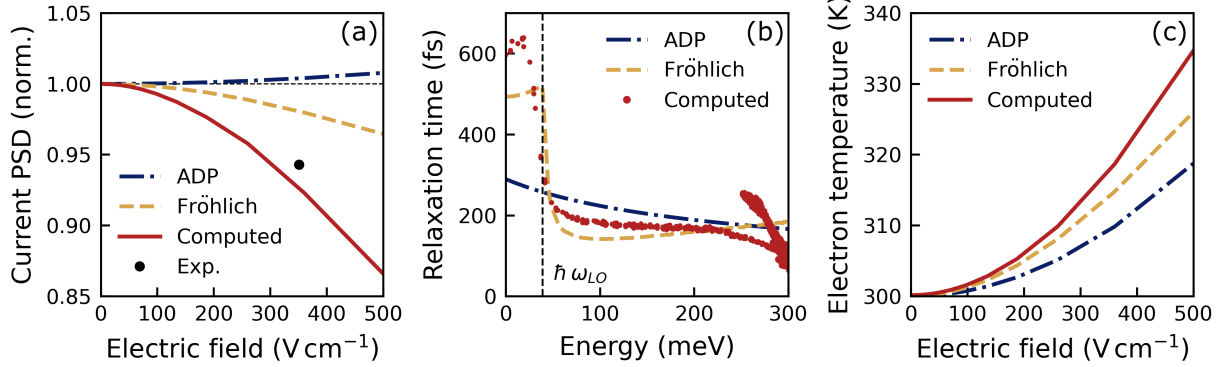


Figure 2. (a) Spectral density of longitudinal current density fluctuations (solid red line) normalized to the Nyquist value versus electric field along with Davydov spectral densities calculated using ADP (dash-dot blue line) and Fröhlich (dashed yellow line). At equilibrium, the noise agrees with Nyquist-Johnson noise (dotted black line). The *ab-initio* calculation predicts a steeper decrease in current PSD with field compared to the approximations. The symbol is an experimental measurement (Figure 11, Ref. [68]). (b) Relaxation times versus energy above conduction band minimum for GaAs at 300 K using ADP (dash-dot blue line), Fröhlich potential (dashed yellow line), and computed (red circles). The energy of the zone-center LO phonon is shown for reference (dashed black line). (c) Effective electron gas temperature versus electric field for ADP (dash-dot blue line), Fröhlich (dashed yellow line), and computed (solid red line). The present calculation predicts more heating than does either approximation.

als need be retained [71]. The zeroth-order term gives the occupancy versus energy and is known as the Davydov distribution. It is given by:

$$F_\epsilon = A \exp \left[ - \int_0^\epsilon \frac{d\epsilon'}{k_B T_0 + 2e^2 \mathcal{E}^2 \tau \tau_\epsilon / 3m} \right] \quad (25)$$

Here  $A$  is a normalizing factor to yield the desired particle number,  $\tau$  is the momentum relaxation time, and  $\tau_\epsilon$  is the energy relaxation time. The model is parametrized by the energy dependence of the momentum and relaxation times and the inelasticity ratio  $\tau/\tau_\epsilon$ . Once these parameters are specified, the Davydov distribution given as Eqn. 25 can be computed and used with Eqn. 20 to calculate the spectral density of current fluctuations [58].

Approximate analytic expressions for the relaxation times in semiconductors are available

[3]. Previous works have calculated the Davydov distribution for a power-law energy dependence of the relaxation times such as that from the acoustic deformation potential (ADP) [72–74]. However, in GaAs at room temperature, the long-ranged Fröhlich interaction with longitudinal optical (LO) phonons is the dominant scattering mechanism [15, 64].

In Fig. 2a, we compare the *ab-initio* longitudinal spectral density to that predicted using the Davydov distribution with the ADP and Fröhlich scattering rates. The approximate relaxation times have been scaled to match the computed low-field mobility, and the inelasticity ratio has been selected using an estimation of the energy and momentum relaxation times (see Fig. 3). The spectral density is observed to decrease monotonically with the electric field. This decrease is captured qualitatively by the Fröhlich calculation. In contrast, the ADP noise increases monotonically with field.

These trends can be understood in terms of the differing energy dependencies of the relaxation times in the various approximations. Figure 2b shows the phonon-mediated relaxation times versus energy for electrons in GaAs at 300 K for the three cases. Below the zone-center LO phonon energy  $\hbar\omega_{LO} \sim 35$  meV, the computed relaxation times are set by LO phonon absorption [14]. Above the LO phonon energy, LO emission becomes dominant and the relaxation times sharply decrease to a value that remains roughly constant until electron energies are near the L-valley minimum at  $\sim 0.25$  eV above the CBM. This absorption-to-emission transition is qualitatively captured by the Fröhlich approximation, although quantitative agreement is poor. The ADP relaxation times agree reasonably well with the computed ones in the emission-dominated region but do not exhibit the absorption-to-emission transition.

The electric field dependence of the spectral noise power reflects the balance between the growth of scattering rates with electron energy and the heating of the electron gas by the DC field. To understand this balance, we examine the effective electron temperature of the steady distribution for the three cases in Figure 2c. The effective electron temperature is calculated as the temperature of a Maxwell-Boltzmann distribution that yields the same energy density as the steady non-equilibrium distribution. At low fields  $\mathcal{E} < 100$  V cm<sup>-1</sup>, the temperature is equal to the lattice temperature. As the electric field increases, the effective temperature increases, corresponding to occupancy at higher energies and increased scattering rates. Near equilibrium where the mobilities are equivalent, the temperature rise predicted from each approximation is similar, but at higher fields, the *ab-initio* calculation

predicts a higher temperature than do either the ADP or Fröhlich approximations.

As the electron gas heats, higher energy states are occupied and thus the spectral noise power, Eqn. 20, includes contributions from fluctuations in those states; hence, the spectral noise power may increase on heating. On the other hand, at these high energies, the scattering events which damp out fluctuations are more frequent, tending to decrease the noise. The competition between these mechanisms sets the trends shown in Figure 2a. For both Fröhlich and the present calculations, the sharp increase in scattering rates associated with the absorption-to-emission transition dominates, and the spectral density decreases monotonically with electric field. In contrast, the ADP approximation shows increasing noise with electric field as the heating of the electrons dominates the weak increase of the scattering rates.

The evolution of the spectral density with electric field demonstrates the sensitivity of the spectral noise power to the energy dependence of the scattering rates. Although the mobility at equilibrium is equivalent for all three cases, the non-equilibrium noise behavior exhibits qualitatively different trends depending on the energy dependence and inelasticity of the scattering mechanisms.

### C. Spectral noise power

The non-equilibrium noise exhibits spectral features that are not present in the Nyquist-Johnson case. Figure 3a shows the spectral density of longitudinal (L) and transverse (T) current fluctuations (relative to the electric field) versus frequency at  $\mathcal{E} = 500 \text{ V cm}^{-1}$ . There are several notable features of the spectral density in this figure. First, the spectral density is constant at low frequencies and rolls off as frequency increases, decreasing to 50% of its low frequency value at 300 GHz. Secondly, an anisotropy exists between the longitudinal and transverse spectral densities. Finally, the longitudinal noise exhibits a non-monotonic trend for frequencies around 50 GHz, similar to that observed for the AC mobility in Fig. 1c. Spectroscopic measurements of the noise power at these frequencies have not been performed, but these trends are qualitatively similar to those observed in recent Monte Carlo simulations [57].

We discuss each of these points in turn. Consider first the noise at equilibrium. The zero-field curve shows that the longitudinal and transverse spectral densities are equal and

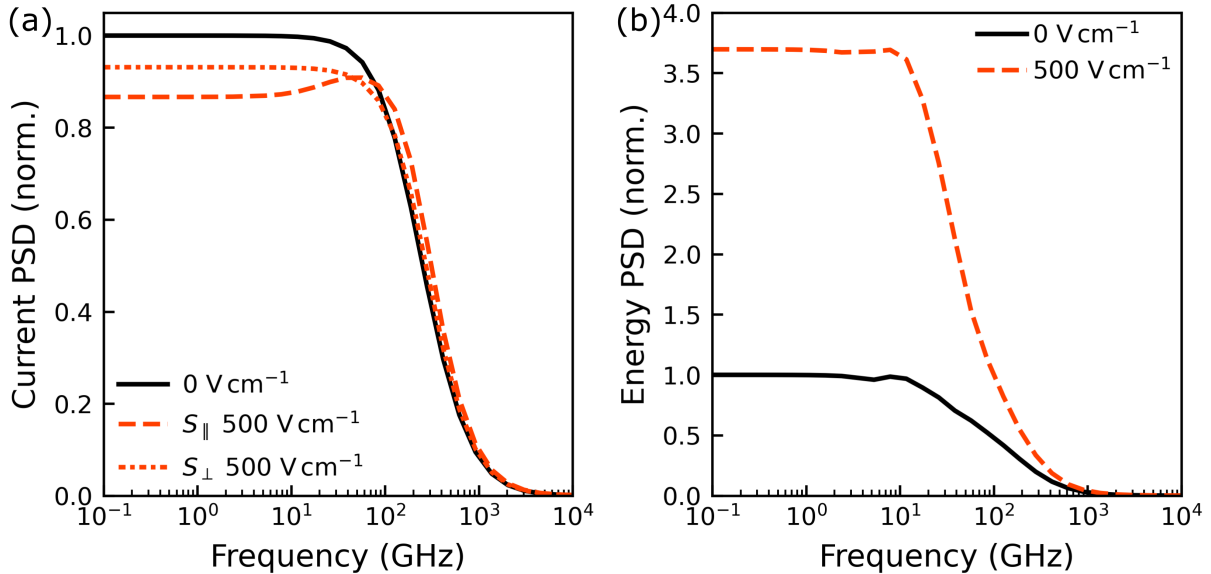


Figure 3. (a) Computed power spectral density (PSD) of longitudinal ( $\parallel$ , dashed orange line) and transverse ( $\perp$ , dotted orange line) current density fluctuations versus frequency at  $\mathcal{E} = 500 \text{ V cm}^{-1}$ , along with the Nyquist-Johnson prediction for  $\mathcal{E} = 0$  (solid black line). (b) Spectral density of energy fluctuations versus frequency at equilibrium (solid black line),  $\mathcal{E} = 500 \text{ V cm}^{-1}$  (dashed orange line). The time scale for electron temperature fluctuations sets the upper frequency limit for the convective mechanism.

coincide with the Nyquist-Johnson value, Eqn. 24. As with the AC mobility, the spectral density rolls off at frequencies exceeding the phonon-mediated scattering rates because the electronic system cannot redistribute in response to the fluctuation. This roll-off behavior has been noted previously [6] and has also been observed for phonon thermal conductivity (see Fig. 1b in Ref. [75]).

Now consider the noise with  $\mathcal{E} = 500 \text{ V cm}^{-1}$ . A similar roll-off with increasing frequency as the equilibrium case is observed. At low frequency, both the longitudinal and transverse spectral densities are lower than the Nyquist value because of the increased electron temperature. However, an anisotropy exists in the spectral densities. The origin of this feature is the 'convective' mechanism [21, 24, 76] and can be understood by decomposing the current fluctuations into two sources. The first is the fluctuation of the drift velocity, induced by stochastic transitions between states of differing group velocity. The second is the fluctuation of the electron temperature, induced by random energy exchange with the

thermal phonon bath. Under non-equilibrium conditions, these fluctuations couple. As the gas is heated by the electric field, the fluctuating current induces a variation in the Joule heating. The resulting electron temperature fluctuation changes the conductivity, which in turn modifies the current. This coupling only exists for fluctuations longitudinal to the electric field because transverse fluctuations do not affect Joule heating. In sublinear CVC materials such as GaAs, the conductivity decreases with electron temperature, and the convective mechanism suppresses longitudinal fluctuations. This feature is indeed observed in Fig. 3a.

The convective mechanism is only present at frequencies  $\omega\tau_\epsilon \ll 1$ , where  $\tau_\epsilon$  is the energy relaxation time. The energy relaxation time can be extracted by calculating the spectral density of electron temperature fluctuations versus frequency. This calculation is the energy analogue of Eqn. 20, where the relevant state quantity is the energy instead of the group velocity. Figure 3b shows the spectral density of energy fluctuations versus frequency for several electric fields. At low frequencies,  $f < 10$  GHz, the spectral density increases with field as the temperature fluctuations rise with higher Joule heating. At higher frequencies,  $f \sim 50$  GHz, the energy fluctuations decrease to 50% of their low frequency values and begin to converge for the two fields shown. This convergence signifies that the temperature of the electron gas cannot change sufficiently rapidly due to its finite thermal capacitance. Consequently, the convective noise mechanism is removed and the anisotropy of the densities in Fig. 3a also disappears; the longitudinal and transverse spectral densities converge. The convective mechanism is also responsible for the non-monotonic trend of the AC mobility seen in Fig. 1c.

#### D. Quasi-elastic scattering

The present formalism for electronic noise permits the study of the microscopic processes responsible for electronic noise in a manner that is difficult to obtain by other methods. As an example, consider the spectral features present in Fig. 3. Comparing the frequency where the current power spectral density and energy power spectral density reach half of their low frequency values (300 GHz versus 50 GHz, respectively), the energy relaxation time is inferred to be around 6 times longer than the momentum relaxation time, implying that the quasi-elastic assumption is valid. This observation is surprising given the well-known

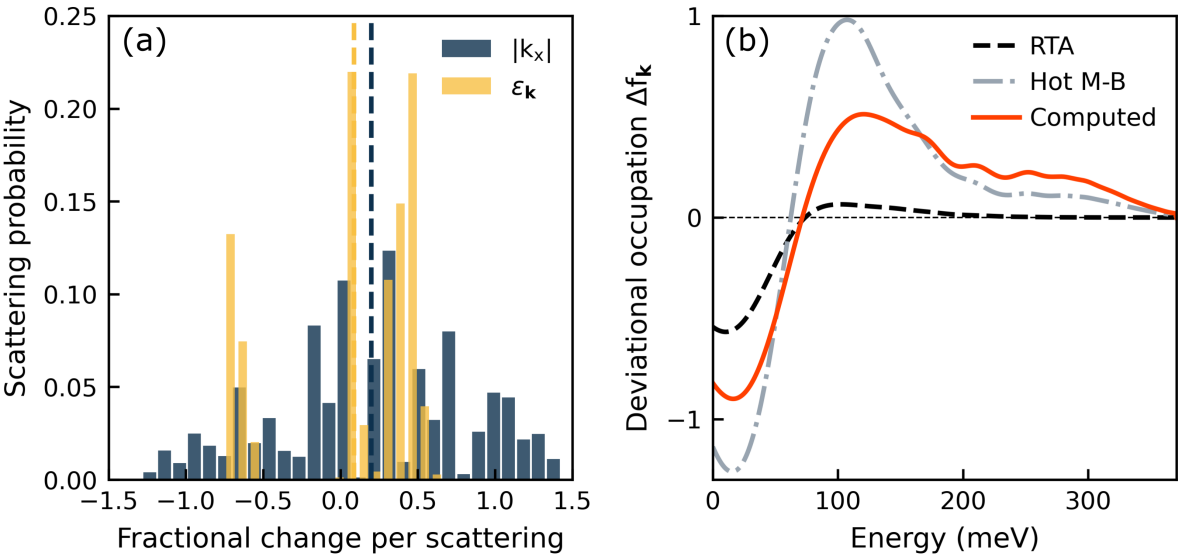


Figure 4. (a) Probability histograms of longitudinal momentum loss  $R_{\mathbf{k}}$  (blue bars) and energy loss  $R_{\epsilon_{\mathbf{k}}}$  (yellow bars) normalized by the thermal averages at  $500 \text{ V cm}^{-1}$ . The dashed lines represent the average transfer per scattering event. At this field, the average fractional dissipation of longitudinal momentum is  $\sim 3\times$  larger than that for energy. (b) Deviational occupation  $\Delta f_{\mathbf{k}}$  in GaAs at 300 K versus energy calculated under the RTA (dashed black line), hot Maxwell-Boltzmann (dashed-dotted grey line), and *ab-initio* warm electron approximation (solid orange line) at  $500 \text{ V cm}^{-1}$ . Neither the RTA nor the Maxwell-Boltzmann capture the hot electron tail.

dominance of high-energy LO phonon emission in GaAs [14] and that inelasticity is expected when the physical temperature is comparable to the Debye temperature [6]. Analytical treatments of noise under dominant LO phonon coupling typically assume strongly inelastic interactions between the electrons and lattice (see Sec. 3.8 of Ref. [24], Sec. 7.3 of Ref. [21], or Ref. [77]).

We identify the origin of this discrepancy by examining how individual scattering events contribute to the momentum and energy relaxation of the electron system to the phonons. These transfers can be expressed as sums over each of the electron-phonon scattering processes in the collision integral weighted by the energy and momentum of the mediating phonon. Every electronic state in the BZ is coupled via phonons to other states; by summing over all possible scattering processes, we obtain the average energy and momentum exchanged in a single scattering event. More precisely, the fractional change in momentum

and energy per scattering event are calculated from:

$$R_{\mathbf{k}} = \frac{1}{\Theta_{\mathbf{kk}} \langle |\mathbf{k}_x| \rangle} \sum_{\mathbf{k}'} (\mathbf{k}_x - \mathbf{k}'_x) \Theta_{\mathbf{k}'\mathbf{k}} \quad (26)$$

$$R_{\epsilon_{\mathbf{k}}} = \frac{1}{\Theta_{\mathbf{kk}} \langle \epsilon \rangle} \sum_{\mathbf{k}'} (\epsilon_{\mathbf{k}} - \epsilon'_{\mathbf{k}}) \Theta_{\mathbf{k}'\mathbf{k}} \quad (27)$$

where  $\langle |\mathbf{k}_x| \rangle$  and  $\langle \epsilon \rangle$  denote the thermal average magnitude of the longitudinal wave vector and electron energy, respectively;  $\Theta_{\mathbf{k}'\mathbf{k}}$  represents the component of the diagonal element of the collision matrix (the scattering rate) corresponding to scattering from  $\mathbf{k}$  to  $\mathbf{k}'$ ; and other variables carry same meaning as defined in Section II.

These fractional changes at  $500 \text{ V cm}^{-1}$  are plotted as a probability histogram in Figure 4a. In this figure, we have binned each state in the BZ by the value of  $R_{\mathbf{k}}$  and  $R_{\epsilon_{\mathbf{k}}}$ . For all the states in a given bin, we calculate the probability of scattering  $\mathcal{P} \propto \sum_{\text{bin}} \Theta_{\mathbf{kk}} f_{m\mathbf{k}}^s$  (the final quantity is normalized to unity). The horizontal position indicates the average fractional change in energy or momentum induced by the event. Positive values of the fractional change correspond to net transfers to the lattice, or dissipation, while negative values correspond to transfers to the electrons, or accumulation. The height of a bar represents the population-weighted probability of scattering in a given time interval.

Figure 4a reveals several important features. First, energy transfers are clustered into two groups. The grouping of accumulation events around  $-0.75$  corresponds to LO absorption, which dominates scattering of electrons below the emission threshold  $\hbar\omega_{LO}$ . The relatively disperse grouping of the dissipation events reflects a balance between LO emission and absorption for states above the threshold. Second, in contrast to energy transfers, momentum transfers grow with the wave vector of the mediating phonon. Consequently, a broader and more disperse distribution of momentum transfers is available. Finally, the balance between dissipation and accumulation differs between energy and momentum. In equilibrium, these processes are balanced, but at  $500 \text{ V cm}^{-1}$ , the net transfers for both quantities are dissipative as the warm electrons transfer excess momentum and energy to the lattice. The dashed lines in the figure represent the average fractional transfer per scattering event and indicate that the net momentum dissipation exceeds the energy dissipation by around a factor of 3. This imbalance is partly responsible for the disparate time scales of energy and momentum relaxation observed in Fig. 3.

The second contributing factor to the relatively long energy relaxation time is the presence of a hot electron tail in the calculated distribution. In Fig. 4b, we plot the steady deviation distribution,  $\Delta f_s$ , calculated under the warm electron approximation using the full  $e\text{-}ph$  scattering matrix versus energy. For reference, the corresponding distributions for a hot Maxwell-Boltzmann at the non-equilibrium electron temperature and a ‘relaxation-time distribution’ obtained under the warm electron approximation with only the on-diagonal elements of the scattering matrix. The *ab-initio* treatment predicts a hot electron tail that is not observed with either approximate method. Although representing only a small fraction of the population, these hot electrons are at energies  $5 - 10\times$  the thermal average value. Consequently, many scattering events are needed to return these electrons to equilibrium, further increasing the energy relaxation time. The result is that the quasi-elastic approximation is unexpectedly accurate despite the inelastic nature of optical phonon scattering, and thus explaining the features in the spectral noise power and AC mobility.

## V. SUMMARY AND FUTURE OUTLOOK

The primary numerical tools used to study electronic noise are Monte Carlo (MC) methods [55–57, 78, 79]. These simulators have many advantages, including the ability to incorporate realistic device geometries and space charge effects through coupled Poisson solvers, and they are thus useful to interpret experimental measurements on devices. However, MC studies rely upon semi-empirical models of scattering and electronic structure that require parameters such as deformation potentials, sound velocities, effective masses, and energy gaps to be specified and calibrated against experiment. The method is thus most useful for well-characterized materials for which these empirical models are available.

A parallel development in the transport field has been the introduction of *ab-initio* methods to study low-field transport phenomena without adjustable parameters. These methods enable not only the computation of low-field transport properties such as electronic mobility [8, 9] and phonon thermal conductivity [80] but also an understanding of the microscopic scattering processes that underlie these macroscopic properties and prediction of the properties of new materials. However, thus far these methods have been restricted to the low-field, cold electron regime.

In this work, we have described an *ab-initio* theory of electronic noise for warm electrons in

semiconductors. The method requires no adjustable parameters, with the phonon dispersion, band structure, and electron-phonon coupling calculated from first-principles. Further, this method permits the study of transport even when the electrons are not in equilibrium with the lattice, being free of the 'cold electron' approximation used in previous transport studies. We demonstrated the method on GaAs, showing that the spectral features of the AC mobility and current noise are linked to the disparate time scales of energy and momentum relaxation, and that the quasi-elastic approximation is unexpectedly accurate despite the dominance of polar optical phonon scattering. Our work paves the way for first-principles studies of electronic noise in semiconductors that will advance the study of transport phenomena and applications of low-noise semiconductor devices.

## ACKNOWLEDGMENTS

The authors thank Jin-Jian Zhou, I-Te Lu, Vatsal Jhalani, and Marco Bernardi, for assistance with PERTURBO and useful discussions. This work was supported by AFOSR under Grant Number FA9550-19-1-0321.

- 
- [1] J.W. Ziman. *Electrons and Phonons: The Theory of Transport Phenomena in Solids*. Oxford University Press, Oxford, 1960.
  - [2] D.K. Ferry. *Semiconductor Transport*. CRC Press, London, 2000.
  - [3] M. Lundstrom. *Fundamentals of Carrier Transport*. Cambridge University Press, Cambridge, 2000.
  - [4] G. Chen. *Nanoscale Energy Transport and Conversion: A Parallel Treatment of Electrons, Molecules, Phonons, and Photons*. MIT-Pappalardo series in mechanical engineering. Oxford University Press, 2005. ISBN 9780195159424. LCCN 2004052066.
  - [5] G.D. Mahan. *Condensed Matter in a Nutshell*. Princeton University Press, Princeton, 2011.
  - [6] Esther Conwell. *High Field Transport in Semiconductors*. Academic Press, 1967. [https://www.google.com/books/edition/{High\\_Field\\_Transport\\_in\\_Semiconductors}/{9teaxQEACAAJ}?hl=en](https://www.google.com/books/edition/{High_Field_Transport_in_Semiconductors}/{9teaxQEACAAJ}?hl=en).
  - [7] Bolin Liao, Jiawei Zhou, Bo Qiu, Mildred S. Dresselhaus, and Gang Chen. Ab initio study

- of electron-phonon interaction in phosphorene. *Phys. Rev. B*, 91:235419, Jun 2015. <https://link.aps.org/doi/10.1103/PhysRevB.91.235419>.
- [8] M. Bernardi. First-principles dynamics of electrons and phonons. *European Physical Journal B*, 89(239), 2016. <https://epjb.epj.org/articles/epjb/abs/2016/11/b160399/b160399.html>.
- [9] Feliciano Giustino. Electron-phonon interactions from first principles. *Rev. Mod. Phys.*, 89: 015003, Feb 2017. <https://link.aps.org/doi/10.1103/RevModPhys.89.015003>.
- [10] Marco Bernardi, Derek Vigil-Fowler, Johannes Lischner, Jeffrey B. Neaton, and Steven G. Louie. Ab initio study of hot carriers in the first picosecond after sunlight absorption in silicon. *Phys. Rev. Lett.*, 112:257402, Jun 2014. <https://link.aps.org/doi/10.1103/PhysRevLett.112.257402>.
- [11] Samuel Poncé, Elena R. Margine, and Feliciano Giustino. Towards predictive many-body calculations of phonon-limited carrier mobilities in semiconductors. *Phys. Rev. B*, 97:121201, Mar 2018. <https://link.aps.org/doi/10.1103/PhysRevB.97.121201>.
- [12] Mattia Fiorentini and Nicola Bonini. Thermoelectric coefficients of *n*-doped silicon from first principles via the solution of the boltzmann transport equation. *Phys. Rev. B*, 94:085204, Aug 2016. <https://link.aps.org/doi/10.1103/PhysRevB.94.085204>.
- [13] Wu Li. Electrical transport limited by electron-phonon coupling from boltzmann transport equation: An ab initio study of si, al, and mos<sub>2</sub>. *Phys. Rev. B*, 92:075405, Aug 2015. <https://link.aps.org/doi/10.1103/PhysRevB.92.075405>.
- [14] Jin-Jian Zhou and Marco Bernardi. Ab initio electron mobility and polar phonon scattering in gaas. *Phys. Rev. B*, 94:201201, Nov 2016. <https://link.aps.org/doi/10.1103/PhysRevB.94.201201>.
- [15] Te-Huan Liu, Jiawei Zhou, Bolin Liao, David J. Singh, and Gang Chen. First-principles mode-by-mode analysis for electron-phonon scattering channels and mean free path spectra in gaas. *Phys. Rev. B*, 95:075206, Feb 2017. <https://link.aps.org/doi/10.1103/PhysRevB.95.075206>.
- [16] N.E Lee, J.J. Zhou, H.Y. Chen, and M. Bernardi. Ab initio electron-two-phonon scattering in gaas from next-to-leading order perturbation theory. *Nature Communications*, 11(1607), 2020. <https://www.nature.com/articles/s41467-020-15339-0>.
- [17] Nien-En Lee, Jin-Jian Zhou, Luis A. Agapito, and Marco Bernardi. Charge transport in

- organic molecular semiconductors from first principles: The bandlike hole mobility in a naphthalene crystal. *Phys. Rev. B*, 97:115203, Mar 2018. <https://link.aps.org/doi/10.1103/PhysRevB.97.115203>.
- [18] V.A. Jhalani, J.J. Zhou, and M. Bernardi. Ultrafast hot carrier dynamics in gan and its impact on the efficiency droop. *Nano Letters*, 17(8), 2017. <https://pubs.acs.org/doi/abs/10.1021/acs.nanolett.7b02212>.
- [19] Jinlong Ma, Arun S. Nissimagoudar, and Wu Li. First-principles study of electron and hole mobilities of si and gaas. *Phys. Rev. B*, 97:045201, Jan 2018. <https://link.aps.org/doi/10.1103/PhysRevB.97.045201>.
- [20] Jifeng Sun, Hongliang Shi, Theo Siegrist, and David J. Singh. Electronic, transport, and optical properties of bulk and mono-layer pdse2. *Applied Physics Letters*, 107(15):153902, 2015. <https://doi.org/10.1063/1.4933302>.
- [21] H.L. Hartnagel, R. Katilius, and A. Matulionis. *Microwave Noise in Semiconductor Devices*. John Wiley & Sons, New York, 2001.
- [22] V Bareikis and R Katilius. *Noise in Physical Systems and 1/f Fluctuations*. WORLD SCIENTIFIC, 1995. <https://www.worldscientific.com/doi/abs/10.1142/2764>.
- [23] E. W. Bryerton, M. Morgan, and M. W. Pospieszalski. Ultra low noise cryogenic amplifiers for radio astronomy. In *2013 IEEE Radio and Wireless Symposium*, pages 358–360. IEEE, 2013. <https://ieeexplore.ieee.org/document/6486740>.
- [24] Sh. Kogan. *Electronic Noise and Fluctuations in Solids*. Cambridge University Press, Cambridge, 1996.
- [25] Herbert B. Callen and Richard F. Greene. On a theorem of irreversible thermodynamics. *Phys. Rev.*, 86:702–710, Jun 1952. <https://link.aps.org/doi/10.1103/PhysRev.86.702>.
- [26] H. Nyquist. Thermal agitation of electric charge in conductors. *Phys. Rev.*, 32:110–113, Jul 1928. <https://link.aps.org/doi/10.1103/PhysRev.32.110>.
- [27] M.A. Leontovich. Fundamental equations of the kinetic theory of gases from the point of view of the theory of random processes. *Zh. Eksp. Teor. Fiz. (JETP)*, 5(3-4), 1935.
- [28] Gregory H. Wannier. Motion of gaseous ions in a strong electric field. ii. *Phys. Rev.*, 87: 795–798, Sep 1952. <https://link.aps.org/doi/10.1103/PhysRev.87.795>.
- [29] N.A. Hashitsume. Statistical theory of nonlinear dissipative systems. *Progress of Theoretical Physics*, 15(4), 1956. <https://academic.oup.com/ptp/article/8/4/461/1857479>.

- [30] B.B. Kadomtsev. Fundamental equations of the kinetic theory of gases from the point of view of the theory of random processes. *Soviet Physics JETP*, 5(4), 1957.
- [31] P. J. Price. Intervalley noise. *Journal of Applied Physics*, 31(6):949–953, 1960. url <https://doi.org/10.1063/1.1735782>.
- [32] Melvin Lax. Fluctuations from the nonequilibrium steady state. *Rev. Mod. Phys.*, 32:25–64, Jan 1960. <https://link.aps.org/doi/10.1103/RevModPhys.32.25>.
- [33] S.V. Gantsevich, V.L. Gurevich, and R. Katilius. Fluctuations in semiconductors in a strong electric field and the scattering of light by "hot" electrons. *Soviet Physics JETP*, 22(4), 1970. <http://www.jetp.ac.ru/cgi-bin/e/index/e/30/2/p276?a=list>.
- [34] Sh.M. Kogan and A.Ya. Shul'man. Theory of fluctuations in a nonequilibrium electron gas. *Soviet Physics JETP*, 29(3), 1969. [https://www.researchgate.net/profile/Alexander\\_Shulman/publication/275659425\\_Theory\\_of\\_Fluctuations\\_in\\_a\\_Noneqilibrium\\_Electron\\_Gas/links/554c0c460cf29f836c990ab6/Theory-of-Fluctuations-in-a-Noneqilibrium-Electron-Gas.pdf](https://www.researchgate.net/profile/Alexander_Shulman/publication/275659425_Theory_of_Fluctuations_in_a_Noneqilibrium_Electron_Gas/links/554c0c460cf29f836c990ab6/Theory-of-Fluctuations-in-a-Noneqilibrium-Electron-Gas.pdf).
- [35] Melvin Lax. Quantum noise. iv. quantum theory of noise sources. *Phys. Rev.*, 145:110–129, May 1966. <https://link.aps.org/doi/10.1103/PhysRev.145.110>.
- [36] K.M. van Vliet and J.R. Fasset. 'fluctuations due to electronic transitions and transport in solids'. In R.E. Burgess, editor, '*Fluctuation Phenomena in Solids*', chapter 7. Academic, New York, 1965.
- [37] Sh.M. Kogan and A.Ya. Shul'man. Extraneous random forces and equations for correlation functions in the theory of nonequilibrium fluctuations. *Soviet Physics Solid State*, 12(4):467, 1970.
- [38] Carlo Jacoboni and Lino Reggiani. The monte carlo method for the solution of charge transport in semiconductors with applications to covalent materials. *Rev. Mod. Phys.*, 55:645–705, Jul 1983. <https://link.aps.org/doi/10.1103/RevModPhys.55.645>.
- [39] L Reggiani, E Starikov, P Shiktorov, V Gruzinskis, and L Varani. Modelling of small-signal response and electronic noise in semiconductor high-field transport. *Semiconductor Science and Technology*, 12(2):141–156, feb 1, 1997. ISSN 0268-1242. <https://iopscience.iop.org/article/10.1088/0268-1242/12/2/001>.
- [40] Christopher J. Stanton and John W. Wilkins. Nonequilibrium current fluctuations in semiconductors: A boltzmann-equation–green-function approach. *Phys. Rev. B*, 35:9722–9734, Jun

1987. <https://link.aps.org/doi/10.1103/PhysRevB.35.9722>.
- [41] Christopher J. Stanton and John W. Wilkins. Hot-electron noise in two-valley semiconductors: An analytic model. *Phys. Rev. B*, 36:1686–1695, Jul 1987. <https://link.aps.org/doi/10.1103/PhysRevB.36.1686>.
- [42] L. Gherardi, A. Pellacani, and C. Jacoboni. Velocity autocorrelation and low temperature mobility of electrons in silicon. *Lettere al Nuovo Cimento*, 14:225–232, 1975.
- [43] R. Fauquembergue, J. Zimmermann, A. Kaszynski, E. Constant, and Greco Microondes. Diffusion and the power spectral density and correlation function of velocity fluctuation for electrons in si and gaas by monte carlo methods. *Journal of Applied Physics*, 51(2):1065–1071, 1980. <https://doi.org/10.1063/1.327713>.
- [44] D. K. Ferry and J. R. Barker. Generalized diffusion, mobility, and the velocity autocorrelation function for high-field transport in semiconductors. *Journal of Applied Physics*, 52(2):818–824, 1981. <https://doi.org/10.1063/1.328421>.
- [45] Tilmann Kuhn, Lino Reggiani, Luca Varani, and Vladimir Mitin. Monte carlo method for the simulation of electronic noise in semiconductors. *Phys. Rev. B*, 42:5702–5713, Sep 1990. <https://link.aps.org/doi/10.1103/PhysRevB.42.5702>.
- [46] L. Varani, L. Reggiani, T. Kuhn, T. Gonzalez, and D. Pardo. Microscopic simulation of electronic noise in semiconductor materials and devices. *IEEE Transactions on Electron Devices*, 41(11):1916–1925, 1994. <https://ieeexplore.ieee.org/document/333807>.
- [47] W. Fawcett and H.D. Rees. Calculation of the hot electron diffusion rate for gaas. *Physics Letters A*, 29(10):578 – 579, 1969. ISSN 0375-9601. <http://www.sciencedirect.com/science/article/pii/0375960169911037>.
- [48] S Bosi and C Jacoboni. Monte carlo high-field transport in degenerate GaAs. *Journal of Physics C: Solid State Physics*, 9(2):315–319, jan 1976. <https://iopscience.iop.org/article/10.1088/0022-3719/9/2/017/pdf>.
- [49] G. Hill, P. N. Robson, and W. Fawcett. Diffusion and the power spectral density of velocity fluctuations for electrons in inp by monte carlo methods. *Journal of Applied Physics*, 50(1): 356–360, 1979. <https://doi.org/10.1063/1.325670>.
- [50] Shulong Wang, Hongxia Liu, Bo Gao, and Huimin Cai. Monte carlo calculation of electron diffusion coefficient in wurtzite indium nitride. *Applied Physics Letters*, 100(14):142105, 2012. <https://doi.org/10.1063/1.3700720>.

- [51] E Starikov, P Shiktorov, V Gružinskis, L Reggiani, L Varani, J C Vaissière, and C Palermo. Monte carlo calculations of hot-electron transport and diffusion noise in GaN and InN. *Semiconductor Science and Technology*, 20(3):279–285, feb 2005. <https://iopscience.iop.org/article/10.1088/0268-1242/20/3/004>.
- [52] R. Rengel and M. J. Martín. Diffusion coefficient, correlation function, and power spectral density of velocity fluctuations in monolayer graphene. *Journal of Applied Physics*, 114(14):143702, 2013. <https://doi.org/10.1063/1.4824182>.
- [53] D Y Xing, M Liu, P Hu, and C S Ting. Diffusion of hot carriers in two-valley semiconductors. *Journal of Physics C: Solid State Physics*, 21(15):2881–2898, may 1988. <https://iopscience.iop.org/article/10.1088/0022-3719/21/15/020>.
- [54] D. Y. Xing, M. Liu, and C. S. Ting. Analytical approach to diffusion of hot carriers in n-type gaas with  $\Gamma$ -l-x band structure. *Phys. Rev. B*, 37:10283–10294, Jun 1988. <https://link.aps.org/doi/10.1103/PhysRevB.37.10283>.
- [55] I. Iñiguez-de-la Torre, J. Mateos, D. Pardo, and T. González. Monte carlo analysis of noise spectra in self-switching nanodiodes. *Journal of Applied Physics*, 103(2):024502, 2008. <https://doi.org/10.1063/1.2832505>.
- [56] H. Rodilla, T. González, D. Pardo, and J. Mateos. High-mobility heterostructures based on inas and insb: A monte carlo study. *Journal of Applied Physics*, 105(11):113705, 2009. <https://doi.org/10.1063/1.3132863>.
- [57] S. Karishy, C. Palermo, G. Sabatini, H. Marinchio, L. Varani, J. Mateos, and T. González. Monte carlo calculation of in0.53ga0.47as and inas noise parameters. In *2017 International Conference on Noise and Fluctuations (ICNF)*, pages 1–4. 'IEEE', 2017. <https://ieeexplore.ieee.org/document/7985941>.
- [58] S.V. Gantsevich, V.L. Gurevich, and R. Katilius. Theory of fluctuations in nonequilibrium electron gas. *Rivista Del Nuovo Cimento*, 2(5), 1979.
- [59] R.H. Fowler. *Statistical Mechanics*. Cambridge University Press, London, 1936.
- [60] Paolo Giannozzi, Stefano Baroni, Nicola Bonini, Matteo Calandra, Roberto Car, Carlo Cavazzoni, Davide Ceresoli, Guido L Chiarotti, Matteo Cococcioni, Ismaila Dabo, Andrea Dal Corso, Stefano de Gironcoli, Stefano Fabris, Guido Fratesi, Ralph Gebauer, Uwe Gerstmann, Christos Gouguassis, Anton Kokalj, Michele Lazzeri, Layla Martin-Samos, Nicola Marzari, Francesco Mauri, Riccardo Mazzarello, Stefano Paolini, Alfredo Pasquarello, Lorenzo Paulatto, Carlo

- Sbraccia, Sandro Scandolo, Gabriele Sclauzero, Ari P Seitsonen, Alexander Smogunov, Paolo Umari, and Renata M Wentzcovitch. QUANTUM ESPRESSO: a modular and open-source software project for quantum simulations of materials. *Journal of Physics: Condensed Matter*, 21(39):395502, sep 2009. <https://iopscience.iop.org/article/10.1088/0953-8984/21/39/395502/meta>.
- [61] P Giannozzi, O Andreussi, T Brumme, O Bunau, M Buongiorno Nardelli, M Calandra, R Car, C Cavazzoni, D Ceresoli, M Cococcioni, N Colonna, I Carnimeo, A Dal Corso, S de Gironcoli, P Delugas, R A DiStasio, A Ferretti, A Floris, G Fratesi, G Fugallo, R Gebauer, U Gerstmann, F Giustino, T Gorni, J Jia, M Kawamura, H-Y Ko, A Kokalj, E Küçükbenli, M Lazzeri, M Marsili, N Marzari, F Mauri, N L Nguyen, H-V Nguyen, A Otero de-la Roza, L Paulatto, S Poncé, D Rocca, R Sabatini, B Santra, M Schlipf, A P Seitsonen, A Smogunov, I Timrov, T Thonhauser, P Umari, N Vast, X Wu, and S Baroni. Advanced capabilities for materials modelling with quantum ESPRESSO. *Journal of Physics: Condensed Matter*, 29(46):465901, oct 2017. <https://iopscience.iop.org/article/10.1088/1361-648X/aa8f79/meta>.
- [62] J. Zhou, J. Park, I. Lu, I. Maliyov, X. Tong, and M. Bernardi. Perturbo: a software package for ab initio electron-phonon interactions, charge transport and ultrafast dynamics. 2020. <https://arxiv.org/abs/2002.02045>.
- [63] J. Sjakste, N. Vast, M. Calandra, and F. Mauri. Wannier interpolation of the electron-phonon matrix elements in polar semiconductors: Polar-optical coupling in gaas. *Phys. Rev. B*, 92: 054307, Aug 2015. <https://link.aps.org/doi/10.1103/PhysRevB.92.054307>.
- [64] Jin-Jian Zhou and Marco Bernardi. Ab initio electron mobility and polar phonon scattering in gaas. *Phys. Rev. B*, 94:201201, Nov 2016. <https://link.aps.org/doi/10.1103/PhysRevB.94.201201>.
- [65] Pauli Virtanen, Ralf Gommers, Travis E. Oliphant, Matt Haberland, Tyler Reddy, David Cournapeau, Evgeni Burovski, Pearu Peterson, Warren Weckesser, Jonathan Bright, Stéfan J. van der Walt, Matthew Brett, Joshua Wilson, K. Jarrod Millman, Nikolay Mayorov, Andrew R. J. Nelson, Eric Jones, Robert Kern, Eric Larson, CJ Carey, İlhan Polat, Yu Feng, Eric W. Moore, Jake VanderPlas, Denis Laxalde, Josef Perktold, Robert Cimrman, Ian Henriksen, E. A. Quintero, Charles R Harris, Anne M. Archibald, Antônio H. Ribeiro, Fabian Pedregosa, Paul van Mulbregt, and SciPy 1. 0 Contributors. SciPy 1.0: Fundamental Algorithms for Scientific Computing in Python. *Nature Methods*, 17:261–272, 2020.

- [66] E. M. Conwell and M. O. Vassell. High-field transport in-type GaAs. *Physical Review*, 166(3):797–821, feb 15, 1968. ISSN 0031-899X. <https://link.aps.org/doi/10.1103/{PhysRev}.166.797>.
- [67] S. Teitel and J. W. Wilkins. Small-signal ac conductivity and velocity overshoot in semiconductor materials. *Journal of Applied Physics*, 53(7):5006–5012, 1982. <https://doi.org/10.1063/1.331376>.
- [68] V. Bareikis, J. Liberis, I. Matulioniene, A. Matulionis, and P. Sakalas. Experiments on hot electron noise in semiconductor materials for high-speed devices. *IEEE Transactions on Electron Devices*, 41(11):2050–2060, 1994. <https://ieeexplore.ieee.org/document/333822>.
- [69] V. Bareikis, K. Kibickas, J. Liberis, A. Matulionis, R. Miliušytė, J. Paršeliūnas, J. Požela, and P. Sakalas. Velocity overshoot and suppression of diffusivity and microwave noise in short n+-n-n+ structures of gaas. In Bengt Källbäck and Heinz Beneking, editors, *High-Speed Electronics*, pages 28–31. Springer Berlin Heidelberg, Berlin, Heidelberg, 1986. ISBN 978-3-642-82979-6.
- [70] V. Bareikis, V. Viktoravicius, A. Galdikas, and R. Miliusyte. Microwave noise and constant of the coupling between the valleys gamma and 1 in a three-valley model of gaas. *Soviet Physics-Semiconductors*, 14(7):847–849, 1980.
- [71] B.J. Davydov. On the theory of electron motion in gases and semiconductors. *Zh. Eksp. Teor. Fiz.*, 8:1069, 1937.
- [72] H R Skullerud. Longitudinal diffusion of electrons in electrostatic fields in gases. *Journal of Physics B: Atomic and Molecular Physics*, 2(6):696–705, June 1969. <https://iopscience.iop.org/article/10.1088/0022-3700/2/6/309>.
- [73] V.L. Gurevich and R. Katilius. Contribution to the theory of hot electrons in an anisotropic semiconductor. *Soviet Physics JETP*, 22:796, April 1966. <http://www.jetp.ac.ru/cgi-bin/e/index/e/22/4/p796?a=list>.
- [74] W.A. Schlup. Definition of noise temperatures  $\theta$  in three dimensions and the conjecture  $\theta \geq t$  in nonequilibrium systems. *Physica*, 69(2):485 – 498, 1973. ISSN 0031-8914. "<http://www.sciencedirect.com/science/article/pii/0031891473900852>".
- [75] Laurent Chaput. Direct solution to the linearized phonon boltzmann equation. *Phys. Rev. Lett.*, 110:265506, Jun 2013. <https://link.aps.org/doi/10.1103/PhysRevLett.110.265506>.

- [76] P.J. Price. 'fluctuations of hot electrons in semiconductors'. In R.E. Burgess, editor, '*Fluctuation Phenomena in Solids*', chapter 8. Academic, New York, 1965.
- [77] R.I. Rabinovich. On galvanomagnetic phenomena under hot-electron energy scattering on optical phonons. *Soviet Physics - Semiconductors*, 3(7):839, 1969.
- [78] H. Rodilla, J. Schleeh, P. Nilsson, N. Wadeffalk, J. Mateos, and J. Grahn. Cryogenic performance of low-noise inp hemts: A monte carlo study. *IEEE Transactions on Electron Devices*, 60(5):1625–1631, 2013. <https://ieeexplore.ieee.org/document/6497570>.
- [79] J. Mateos, H. Rodilla, B.G. Vasallo, and T. Gonzalez. Monte carlo mmodelling of noise in advanced iii-v hemts. *Journal of Computational Electronics*, 14:72–86, 2015. <https://link.springer.com/article/10.1007/s10825-014-0653-1>.
- [80] L. Lindsay, C. Hua, X.L. Ruan, and S. Lee. Survey of ab initio phonon thermal transport. *Materials Today Physics*, 7:106 – 120, 2018. ISSN 2542-5293. <http://www.sciencedirect.com/science/article/pii/S254252931830141X>.